water

MDPI

Article

An Experimental Study of Flow and Turbulence Properties near the Rising Sector Gate Mouth Considering the Gate Opening with a PIV Measuring System

Chang Geun Song [1], Sung Won Park [2,*] and Jaehyun Shin [3]

[1] Department of Safety Engineering, Incheon National University, 119, Academy-ro, Yeonsu-gu, Incheon 22012, Republic of Korea; baybreeze119@inu.ac.kr
[2] Department of Civil and Environmental Engineering, Incheon National University, 119, Academy-ro, Yeonsu-gu, Incheon 22012, Republic of Korea
[3] Department of Civil and Environmental Engineering, Gachon University, 1342, Seongnam-daero, Sujeong-gu, Seongnam-si 13120, Republic of Korea; jaehyunshin@gachon.ac.kr
* Correspondence: s.w.park@inu.ac.kr; Tel.: +82-32-835-8466

Abstract: Hydraulic structures, such as movable weir gates, are widely installed in rivers and streams for various purposes. Among these is the rising sector gate, which is the focus of this study. This research investigated how different gate openings affect flow velocity and turbulence distributions at the gate mouth. A hydraulic analysis of flow and turbulence characteristics near the mouth of a rising sector gate model was conducted through laboratory experiments with various flow conditions and gate openings utilizing a Particle Image Velocimetry (PIV) system. Experimental tests were carried out with two gate-opening angles (30 and 45 degrees). The PIV measurements revealed significant variations in flow velocity and turbulence properties in response to the gate openings and flow conditions. Notably, in the vicinity of the gate mouth, where the flow regime changes rapidly between the upstream and downstream regions, the turbulence properties in the upstream part of the gate mouth were more than twice those in the downstream part. Additionally, the streamwise distribution of depth-averaged relative turbulence intensity was analyzed. The results showed that the depth-averaged relative turbulence intensity decreased by nearly half as the gate opening increased from 30 to 45 degrees, with the lowest values observed at the gate mouth, followed by an increase downstream. A functional relationship between the maximum flow velocity at the gate mouth during underflow operation and the Froude number was established to guide practical gate operation in the field.

Keywords: hydraulic structures; rising sector gate; gate opening; particle image velocimetry (PIV); velocity distribution; turbulence intensity; depth-averaged relative turbulence intensity

Citation: Song, C.G.; Park, S.W.; Shin, J. An Experimental Study of Flow and Turbulence Properties near the Rising Sector Gate Mouth Considering the Gate Opening with a PIV Measuring System. *Water* **2024**, *16*, 3004. https://doi.org/10.3390/w16203004

Academic Editor: Mohamad Basel Al Sawaf

Received: 5 September 2024
Revised: 15 October 2024
Accepted: 16 October 2024
Published: 21 October 2024

1. Introduction

Currently, South Korea, along with the rest of the world, is experiencing more frequent droughts and floods, primarily due to climate change and uncontrolled industrialization. These events have led to increasing damages to both property and human life. Moreover, critical issues like water shortages and the pollution of rivers and streams require urgent attention. Since 2008, the Four Major Rivers Restoration Project has been underway, aiming to enhance the environmental quality around the rivers, which had been previously neglected, and to tackle water-related problems stemming from climate change. A significant aspect of this restoration project involves the construction of 16 multi-purpose weirs in the four major river basins. These weirs are expected to ensure stable water surface elevation, sufficient water discharge, an eco-friendly environment, and sustainable ecological habitats. However, despite the evaluation of their effectiveness and the use of scaled physical and numerical modeling for the weir gates' design, various damages and problems have arisen during the flood season

in the developed river basins. These issues include scour problems downstream of weir gates, head cutting in confluences, and partial collapses of hydraulic structures. Furthermore, inappropriate operations and maintenance of weir gates and other structures have accelerated ecological problems and habitat difficulties. Consequently, engineering solutions and sustainable efforts are urgently required to overcome these challenges. In particular, improvements in the structural design of weir gates and sub-structures are necessary. Numerous previous studies have addressed this topic, particularly employing various measuring apparatuses and practical approaches. Experimental investigations have provided detailed and consistent information on the statistical properties of turbulence in open-channel flows and boundary layer flows. While PIV has been widely used to provide spatial information on turbulent flow, its capability to provide distributions of time-averaged turbulence quantities, especially those involving high-order moments such as skewness or turbulent kinetic energy, requires further investigation [1]. And, a previous study presented different approaches for the flow of sluice gates [2]. The use of sluice gates as discharge-measuring structures is found in the work of Rajaratnam and Subramanya [3]. Numerous studies have been reported in the literature concerning the flow over weirs, including those by Ackers et al. [4] and Swamee [5]. Specifications and proper installation methods for weirs for flow measurements have been discussed by BSI [6] and USBR [7–9]. Additionally, studies have examined the characteristics of scour holes downstream of combined free flow over weirs and below gates [10]. The rising occurrence of these events has prompted increased research interest in developing new risk analysis methods for preventing and mitigating potential harm to people, the natural environment, and industrial facilities. The concept of multi-hazard involves the combination of two or more threat factors occurring in an isolated, simultaneous, or chain reaction manner, leading to a triggering disaster event. Therefore, we tried to conduct a comprehensive review of the design documents and standards related to riverbed protection. Specifically, we focused on examining standards that incorporate and reflect the hydraulic characteristics of the river and evaluate those structures' performance. In this study, we employed a physical laboratory experimental approach to analyze the hydrodynamics of the flushing operation of the rising sector gate, focusing on its impact on water flow and sediment management.

2. Research Background

2.1. Gated Weir Flow

The types of weirs in rivers and streams can be classified as fixed and movable weirs. The movable weir, due to its diversity in water level control, is commonly installed and operated for various purposes. A roller gate is one of the most commonly applied types of movable weir and is classified with four kinds of operations in the field. Schematics of these are provided in Figure 1. The operation of a roller gate involves four key flow regimes: Figure 1a shows free weir flow, where water freely flows over the weir when the upstream water level is higher than the downstream level, and the downstream level does not submerge the weir; Figure 1b shows submerged weir flow, which occurs when the downstream water level is high enough to partially or fully submerge the weir, thereby restricting the flow; Figure 1c shows free orifice flow, where water flows freely through the gate opening when the gate is partially open, and the downstream level is lower, allowing unobstructed flow; and Figure 1d shows submerged orifice flow, which happens when the downstream water level is high enough to submerge the gate opening, restricting the flow through the orifice. Each of these is crucial for effective water level management and flood control.

The overflow of the weir floor usually has large values of energy and velocity. Therefore, to protect the bed structures of weirs and their downstream areas, many kinds of engineering designs have been applied. Recently, design techniques for movable weir gates have been developed and applied in the field. Newly designed weir gates can continuously remove the sediment upstream and flexibly control the water surface elevation. However, most of them have only focused on improving the function and shape of the weir gate, and the bed structures have been designed with classical design methods. Even though

financial and physical advantages could be obtained with new techniques, a lot of problems and weaknesses in designing movable weir gates and structures still remain. Flow changes can be induced by varying upstream or downstream discharge, as well as by routine gate operation. In general, four types of flows can be observed at the gate. Each of the four regimes has a unique equation, and the flow can transition from one regime to another. In the design of underflow gates such as sluice, tainter, and roller gates, hydraulic engineers prioritize understanding the head–discharge relationship and pressure distribution across the gate surfaces. The design of the gate lip is critical, as it impacts the flow behavior and can cause undesirable vibrations if not properly configured [11].

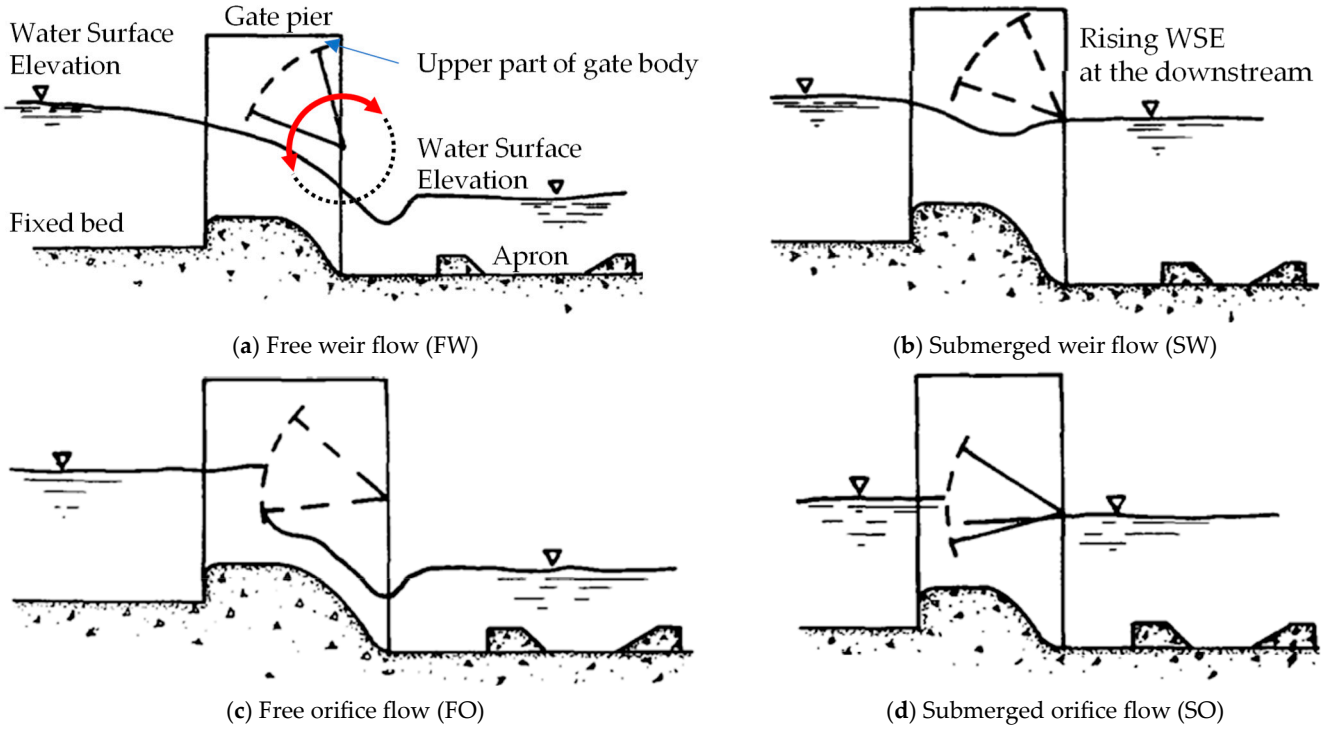

(**a**) Free weir flow (FW)

(**b**) Submerged weir flow (SW)

(**c**) Free orifice flow (FO)

(**d**) Submerged orifice flow (SO)

Figure 1. Schematics of gated weir flow (revised from [11]).

There are many types of movable weir gates, with the rising sector gate being increasingly popular in recent years due to its versatility and effectiveness [12–17]. Most of the previous studies proposed functional relationships between hydraulic parameters and specific coefficients, such as discharge coefficients. However, there have been no studies that have conducted a detailed analysis of the precise velocity or turbulent behavior related to gate operation. This gate is particularly favored for its ability to provide precise control over water flow, making it suitable for a variety of applications, such as flood management, sediment flushing, and water level regulation. A rising sector gate operates by rotating on a horizontal axis, allowing it to control the water flow by raising or lowering the gate. This design offers efficient and flexible water management, especially in environments where accurate flow control is critical (Figure 2). Therefore, depending on the gate operation method, particularly for the undershot operation, which can flush out sediments accumulated in the upstream section, it is necessary to analyze the flow and turbulent properties when the lower part of the gate is partially opened.

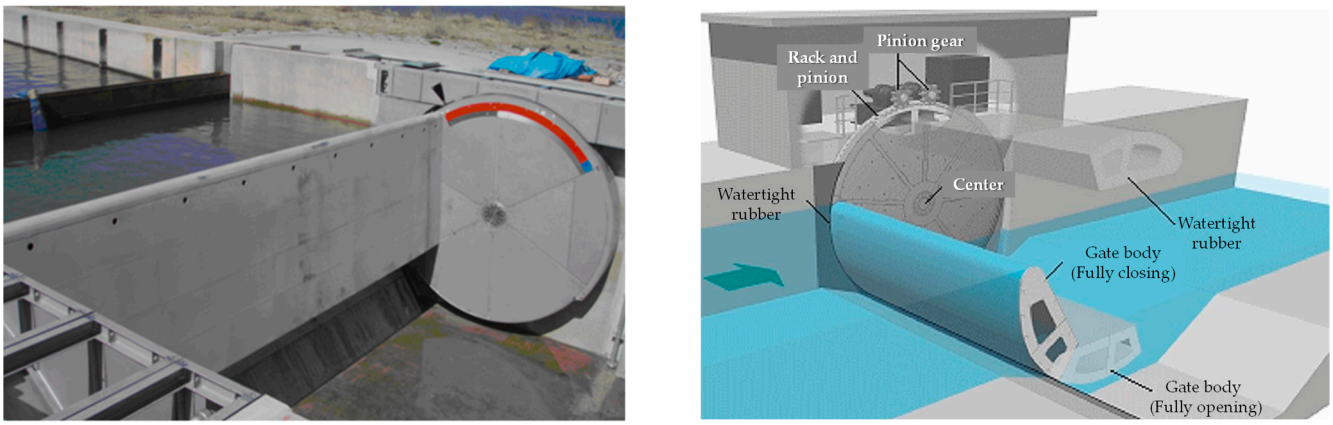

(**a**) On-site (**b**) Schematic diagram

Figure 2. Photos of rising sector gate.

The rising sector gate also operates in four distinct flow regimes based on those of a gated weir flow (Figure 3). In Figure 3a, the gate is fully lowered and locked in place for safe maintenance and inspection operations. In the fully open position of a gated flow system, when the gate is completely open, resulting in no step difference, a hydraulic jump can occur, which can enhance oxygen aeration. Figure 3b shows the flood control position, where the gate is fully closed to the upstream direction, effectively blocking water flow to control upstream water levels. Figure 3c illustrates the undershot flow position or flushing, where the gate remains in the flood control position but is slightly raised at the bottom, allowing water to flow underneath and flush out sediments accumulated upstream, which is the type focused on in this study. Finally, Figure 3d depicts the maintenance position, where the gate is lifted entirely upward, enabling water to flow freely beneath it while allowing for inspection or maintenance of the gate structure.

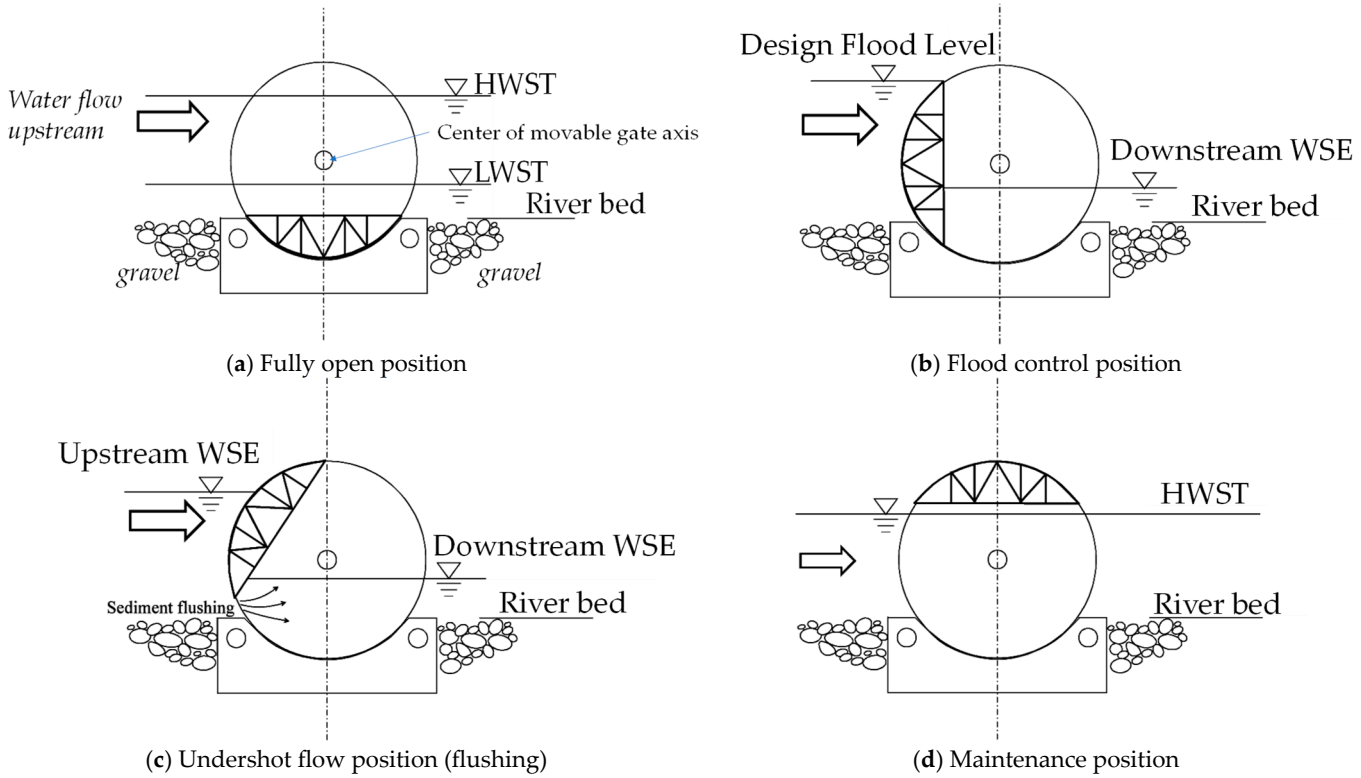

(**a**) Fully open position (**b**) Flood control position

(**c**) Undershot flow position (flushing) (**d**) Maintenance position

Figure 3. Types of rising sector gate operation.

2.2. Flow and Turbulence

There are various methods for considering flow and turbulence properties. However, one approach to quantifying and analyzing these properties across an entire area is to calculate the depth-averaged relative turbulence intensity (r_0). r_0 is particularly useful as it can be directly applied in the field with no scale effects [18,19]. It can be calculated as follows:

$$r_0 = \sqrt{k_0}/U_0 \tag{1}$$

where k_0 and U_0 are the depth-averaged turbulence energy per unit mass and depth-averaged flow velocity, respectively. k_0 can be integrated from the depth-wise directional distribution of turbulent kinetic energy per unit mass (k) as follows:

$$k_0 = \frac{1}{h}\int_0^h k(z)dz \tag{2}$$

where h is the water depth, and k is the mean turbulent kinetic energy per unit mass associated with eddies in turbulent flow. z denotes the depth-wise directional location. k can be calculated through the summation of three-dimensional turbulence intensity as follows:

$$k = \frac{1}{2}\left(\overline{u'^2} + \overline{v'^2} + \overline{w'^2}\right) \tag{3}$$

The three terms related to flow fluctuation on the RHS of Equation (3) are calculated as follows:

$$\overline{u'^2} = \overline{(u - \overline{U})^2} \tag{4}$$

$$\overline{v'^2} = \overline{(v - \overline{V})^2} \tag{5}$$

$$\overline{w'^2} = \overline{(w - W)^2} \tag{6}$$

where u, v, and w are instantaneous flow velocities in the streamwise, width-wise, and depth-wise directions, respectively. Additionally, the apostrophe and overbar denote the properties of the flow fluctuation and time-averaging, respectively.

The Reynolds shear stress represents the shear stress arising from turbulence in the fluid flow and is calculated using the time-averaged values of the fluctuating velocity components. This is a key factor used in this study for analyzing the turbulent components of gated flow in undershot operation. Based on the decomposition of the three-dimensional flow velocity distribution, the Reynolds shear stress in the x-z plane is calculated using the following equation:

$$\tau_{xz} = -\rho_w \overline{u'w'} \tag{7}$$

where τ_{xz} is the Reynolds shear stress in the x-z plane, ρ_w is the water density, and $\overline{u'w'}$ is the time-averaged product of the fluctuating velocity components in the x- and z-directions.

3. Laboratory Experiments

3.1. Model Setup

Laboratory experiments for this research were conducted in a glass-walled flume. The flume has overall dimensions of 17.5 m in length, 0.6 m in width, and 0.8 m in depth. A head tank, measuring 2.9 m in length, 1.2 m in width, and 1.5 m in height, was connected to the upstream end of the channel to stabilize the water supply. Two honeycomb screens were installed within the head tank. The side walls and part of the channel bottom were constructed from 8 mm and 12 mm thick glass, respectively. Notably, the transparent glass bottom allowed a laser sheet to be projected from below the flume. The flume was reinforced and supported by a painted steel framework. The open channel for measurement had dimensions of 15.0 m in length, 0.6 m in width, and 0.8 m in depth. At the downstream end, a steel sluice gate was installed to control the water surface elevation (Figures 4 and 5).

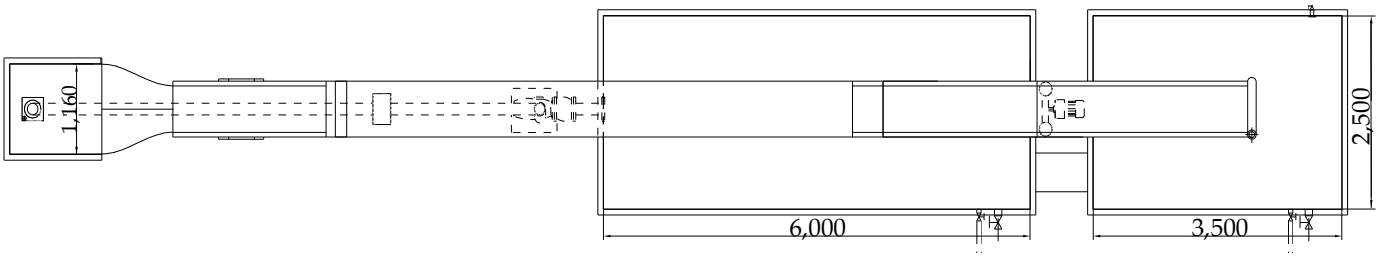

(**a**) Plan view

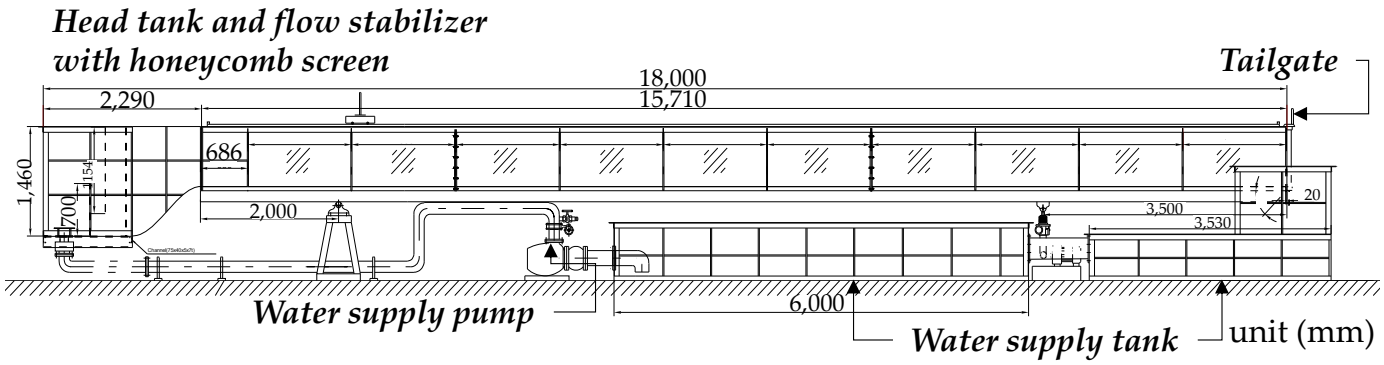

(**b**) Side view

Figure 4. Design of experimental channel and water supply system.

(**a**) Front view of head tank

(**b**) Side view of head tank

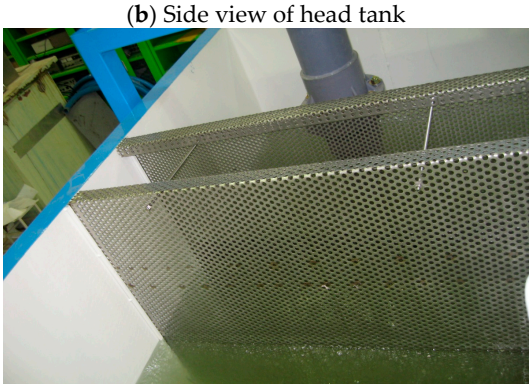

(**c**) Honeycomb screens in head tank

Figure 5. Photos of experimental flume (inlet part).

The water discharge for the experiments operates in a fully recirculating system as follows: Water from the first water supply tank is pumped through a trumpet-shaped suction pipe by the water supply pump. An ultrasonic flowmeter (Ultraflux Co., Ltd., Yerres, France) is installed in the middle of the water supply pipe to monitor the flow

rate based on the experimental condition. A perforated pipe installed in the head tank ensures a stable water discharge through a pair of honeycomb screens and low weirs. After passing through the channel, the water is collected in the second water supply tank and then delivered back to the first water supply tank via a connecting rectangular culvert positioned 0.5 m above the tank bottom. This experimental setup features a recirculation system where the water that passes through the tailgate, installed downstream to maintain the water surface elevation, is recycled in two water supply tanks located beneath the flume. The recycled water is then pumped back to the head tank by a water supply pump (Figures 4–6).

(**a**) Tailgate at the flume downstream

(**b**) Water supply pump

(**c**) Control panel with display

Figure 6. Photos of outlet part and water supply system.

3.2. Measuring Apparatus and Gate Model

For visualization of the flow near the weir gate, four components were utilized. The laser source was a 135 mJ dual NdYAG operating at a wavelength of 532 nm with a pulse rate of 15 Hz. Various laser light sheet optics were employed to spread the laser beam. A digital camera with a 2-megapixel resolution was used to capture fluid motion, providing a relatively large interrogation area. All components were synchronized using a synchronizer to coordinate the capture commands and image acquisition (Figure 7, Appendix A).

For PIV measurement, a laser injector, synchronizer, CCD camera, and optic lens are required. The pulse laser generator consists of two laser heads and provides stable, high output without calibration, and the optic lens is a device that creates a laser sheet by attaching or detaching from the head of the laser injector and allows accurate irradiation of the fluid to be measured. The synchronizer is a device that synchronizes the operation of the pulse laser and CCD camera and adjusts the cycle of signal processing (Figure A1 in Appendix A).

The experiment was conducted using the PIV measuring system installed alongside the experimental channel and water supply system described in Section 3.1. As shown in Figure 8, when water flows through the flume, the laser sheet is refracted in the perpen-

dicular direction to measure the two-dimensional vertical flow behavior (x-z) within the channel. To avoid the influence of water surface fluctuations, a tempered glass channel bottom was installed in the analysis area, allowing the laser sheet to be scanned from the bottom of the flume toward the water surface (Figure 8). The coordinates of the CCD camera are controlled by an auto-traverse device mounted on the carriage, which can be operated via a PC (Figure A2 in Appendix A).

(**a**) Laser injector

(**b**) Synchronizer

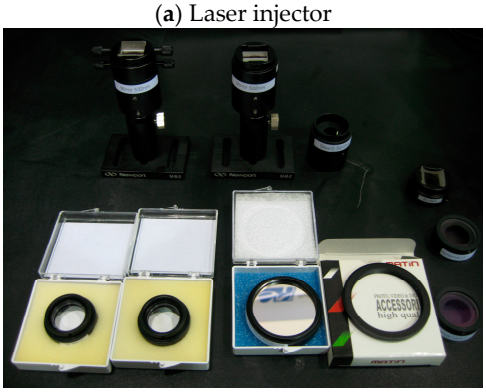

(**c**) CCD camera

(**d**) Lens filter

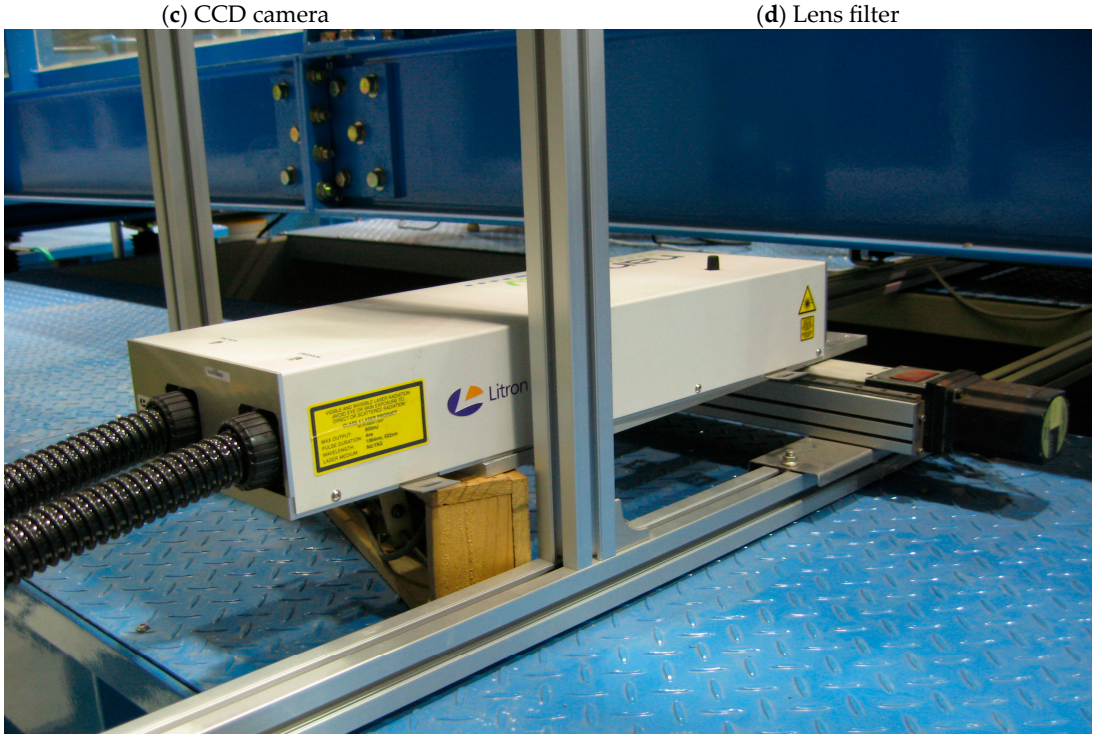

(**e**) Laser injector on the traverse

Figure 7. Photos of PIV measuring system.

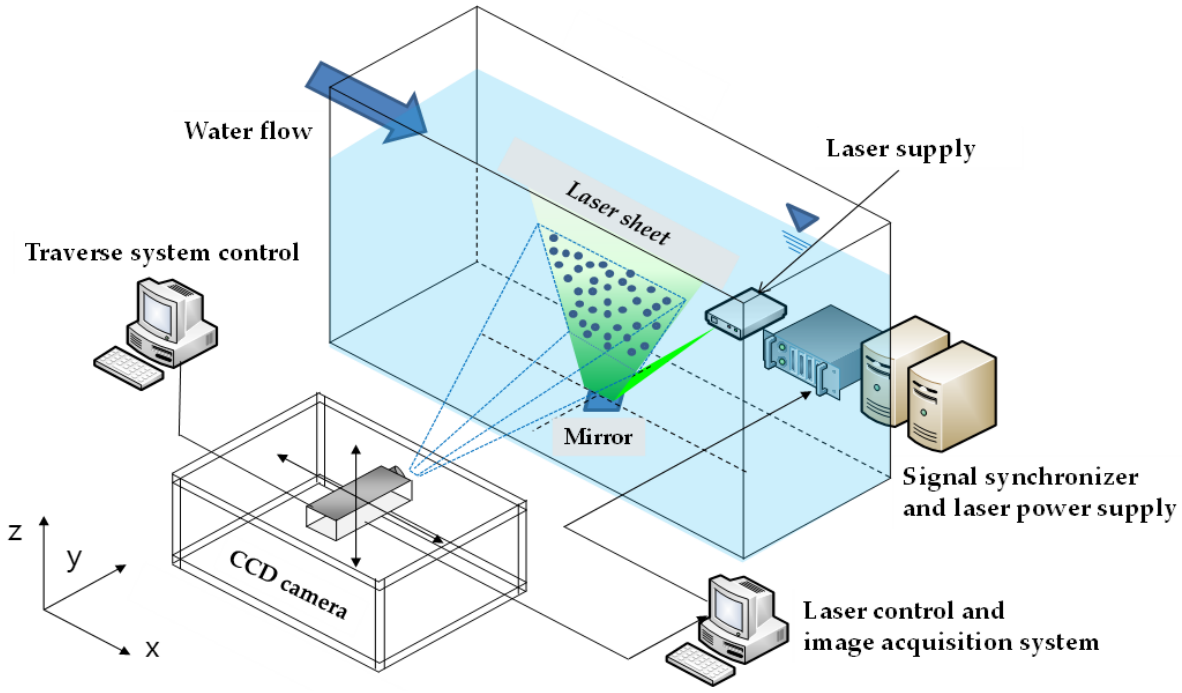

Figure 8. Schematics of PIV measuring system in the experimental channel.

The total length of the gate model is approximately 1000 mm, with a width of 450 mm. The gate section was manufactured with an arc length of 150 mm, and all components, including the pier section, were made of acrylic to maximize the transmittance of the laser sheet. The interior was designed to be hollow. The gate model was constructed to allow for complete opening, complete closing, and partial opening at angles of 30°, 45°, and 60°. The inlet and outlet of the gate section, where the gate is connected, were designed with sine-curved surfaces to ensure the smooth inflow and outflow of the supply water, and the bottom surface of the inlet was shaped into a wedge to stabilize the water flow upstream (Figures 9 and 10).

Images captured with a CCD camera using the PIV measurement method can be more easily post-processed using Insight3G v8.1, a specialized image post-processing software. The velocity data files (*.vec) acquired over time can be used to calculate various velocity and turbulence parameters using Tecplot 360 EX 2023 R and Matlab-2024a, which are integrated into Insight3G v8.1. Tecplot includes built-in functions that can calculate factors such as Reynolds stress distribution, turbulence intensity, and vorticity distribution over time, and it is designed to be easily operated on Windows without the need to modify the internal code. Matlab-2024a allows users to extract and save the velocity changes at specific points of interest over time as data files.

In this study, the data for each experimental condition were acquired with a sampling rate of 10 Hz for 50 s, resulting in the analysis of 500 images, considering previous research [20–24]. The time-averaged velocity and fluctuating flow components were then calculated. The measurement area for this experiment was set to 160 mm in the flow direction (x-direction) and 120 mm in the water depth direction (z-direction). The section covered by the gate model was excluded from the post-processing grid. The gate was considered completely closed at 0°, and experiments were conducted with the gate partially opened at angles of 30° and 45° toward the upstream direction.

In this study, the flow and turbulence properties were analyzed during the undershot operation, or flushing operation, which is one of the four flow regimes of the rising sector gate. The experiment was conducted under 12 different conditions, using varying upstream supply flow rates (Q_u = 0.003, 0.006, and 0.010 m^3/s), two downstream water levels (h_d = 0.355 m and 0.400 m), and two gate-opening angles (30° and 45°) (Table 1).

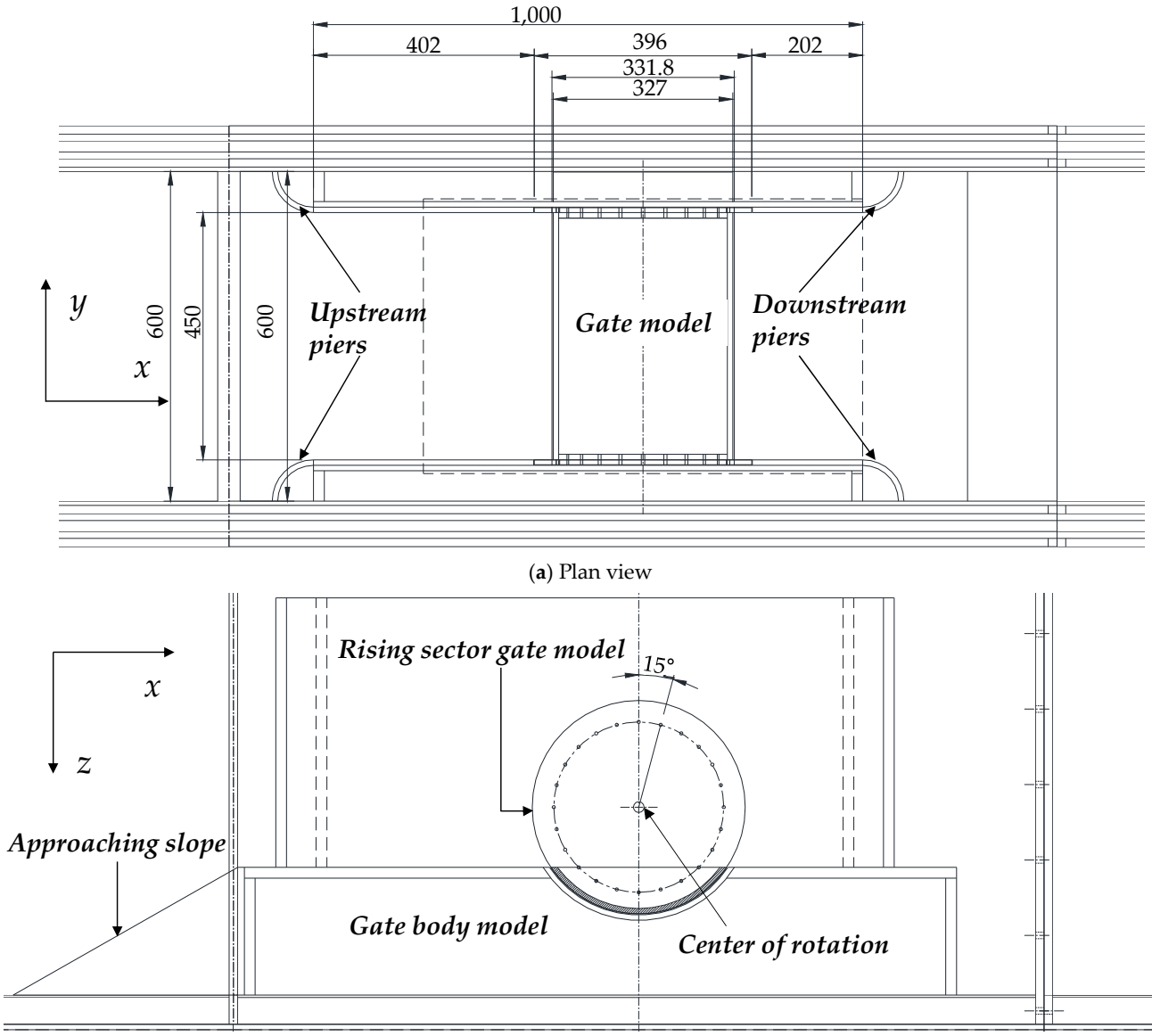

(**a**) Plan view

(**b**) Side view

Figure 9. Design of rising sector gate model.

Table 1. Experimental conditions.

Gate Opening (Degree)	Case Number	Q_u (m^3/s)	h_u (m)	h_d (m)	Fr (-)
30	FO1_101	0.003	0.360	0.355	0.00755
	FO1-201	0.006	0.385		0.01510
	FO1-301	0.010	0.415		0.02516
	FO1-102	0.003	0.410	0.400	0.00631
	FO1-202	0.006	0.428		0.01262
	FO1-302	0.010	0.483		0.02103
45	FO2-101	0.003	0.355	0.355	0.00755
	FO2-201	0.006	0.360		0.01510
	FO2-301	0.010	0.370		0.02516
	FO2-102	0.003	0.402	0.400	0.00631
	FO2-202	0.006	0.405		0.01262
	FO2-302	0.010	0.407		0.02103

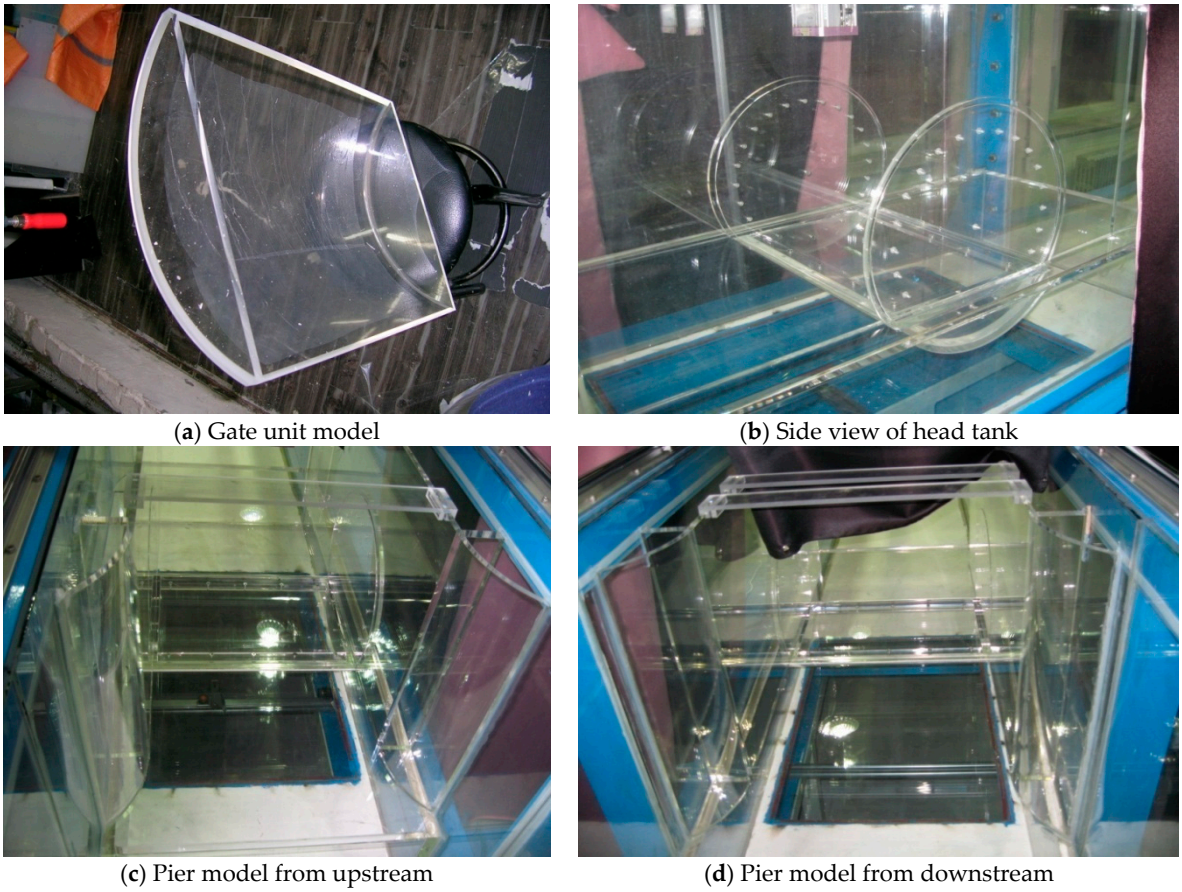

(**a**) Gate unit model (**b**) Side view of head tank

(**c**) Pier model from upstream (**d**) Pier model from downstream

Figure 10. Photos of acrylic model of weir gate.

4. Results

4.1. Time-Averaged Flow Velocity Distribution

A total of 500 data sets were acquired at a sampling rate of 10 Hz, and the time-averaged velocity profiles are presented in Figures 11 and 12 for gate openings with 30 and 45 degrees. The flow patterns upstream of the weir gate are relatively stable, while the downstream flow tends to circulate back toward the upstream as the upstream discharge and downstream water surface elevation increase. Localized vortices are observed near the boundary of the weir gate. The velocity at the gate opening exceeds approximately twice the cross-sectional averaged velocity.

Under the upstream water discharge condition of 0.003 m^3/s, the maximum velocity occurs at the lower discharge section of the gate, with the exception of localized eddy formations. Additionally, as the upstream water discharge increases, the velocity shows a slight increase compared to the 0.003 m^3/s condition. Notably, the velocity at the boundary between the gate mouth and the upstream section is significantly higher. This velocity distribution is expected to increase the shear stress on the gate structure, potentially contributing to structural damage and degradation. When the flow rate is 0.010 m^3/s, a prominent backward flow pattern emerges in the downstream section of the sluice gate. This is likely due not only to the velocity deviation from the upper layer as water passes through the open section of the gate but also to the influence of the arc-shaped water receiver downstream of the gate. Figure 12 illustrates the velocity distribution when the sluice gate is opened at 45°. The results indicate that the height of the outlet at the open sluice gate more than doubled compared to the 30° opening, while the average discharge velocity decreased. Additionally, it was observed that the tendency for the velocity to flow downward along the upstream boundary of the gate diminished significantly when the downstream water level was increased.

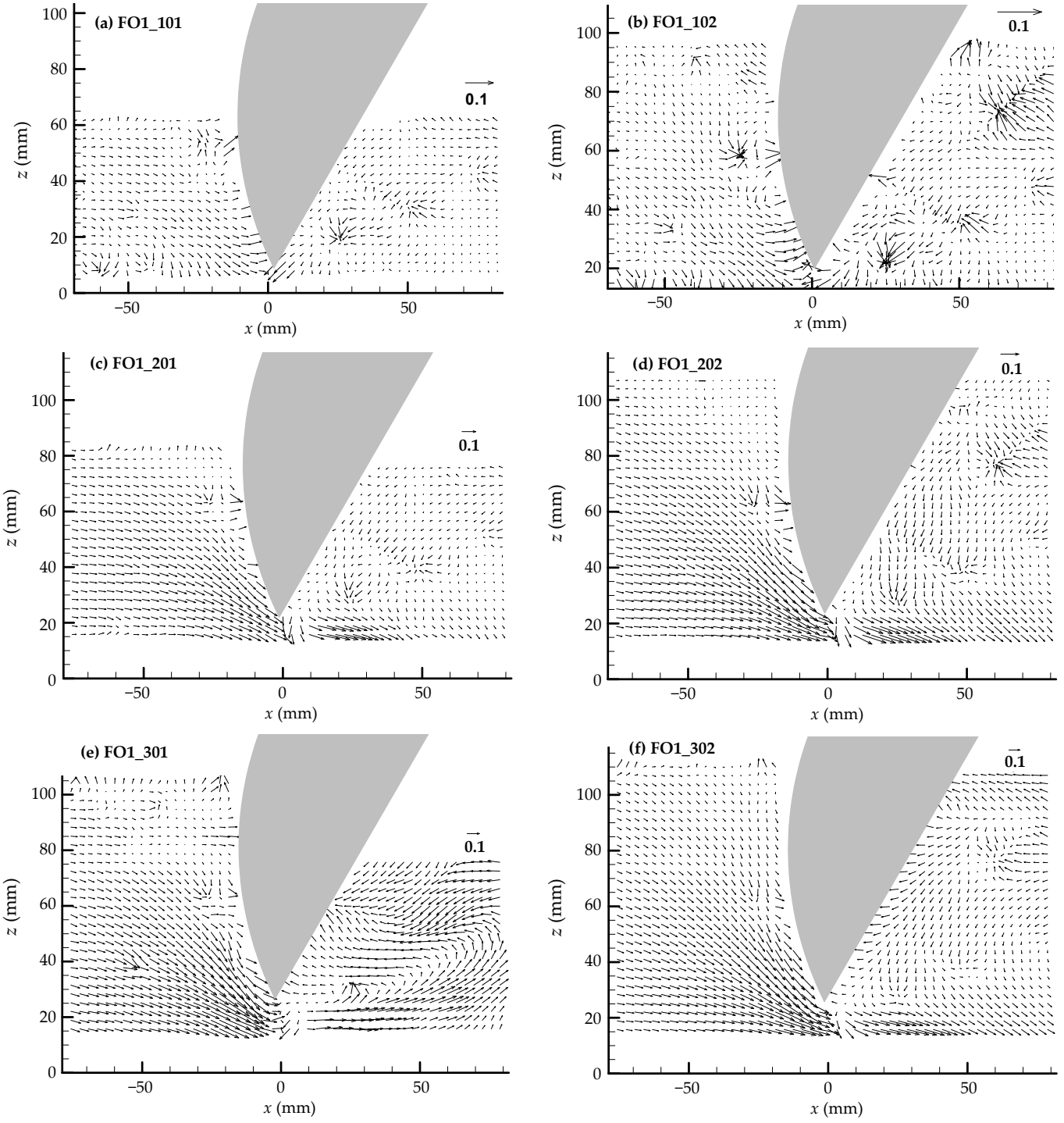

Figure 11. Two-dimensional vector plots near the weir gate mouth (case FO1).

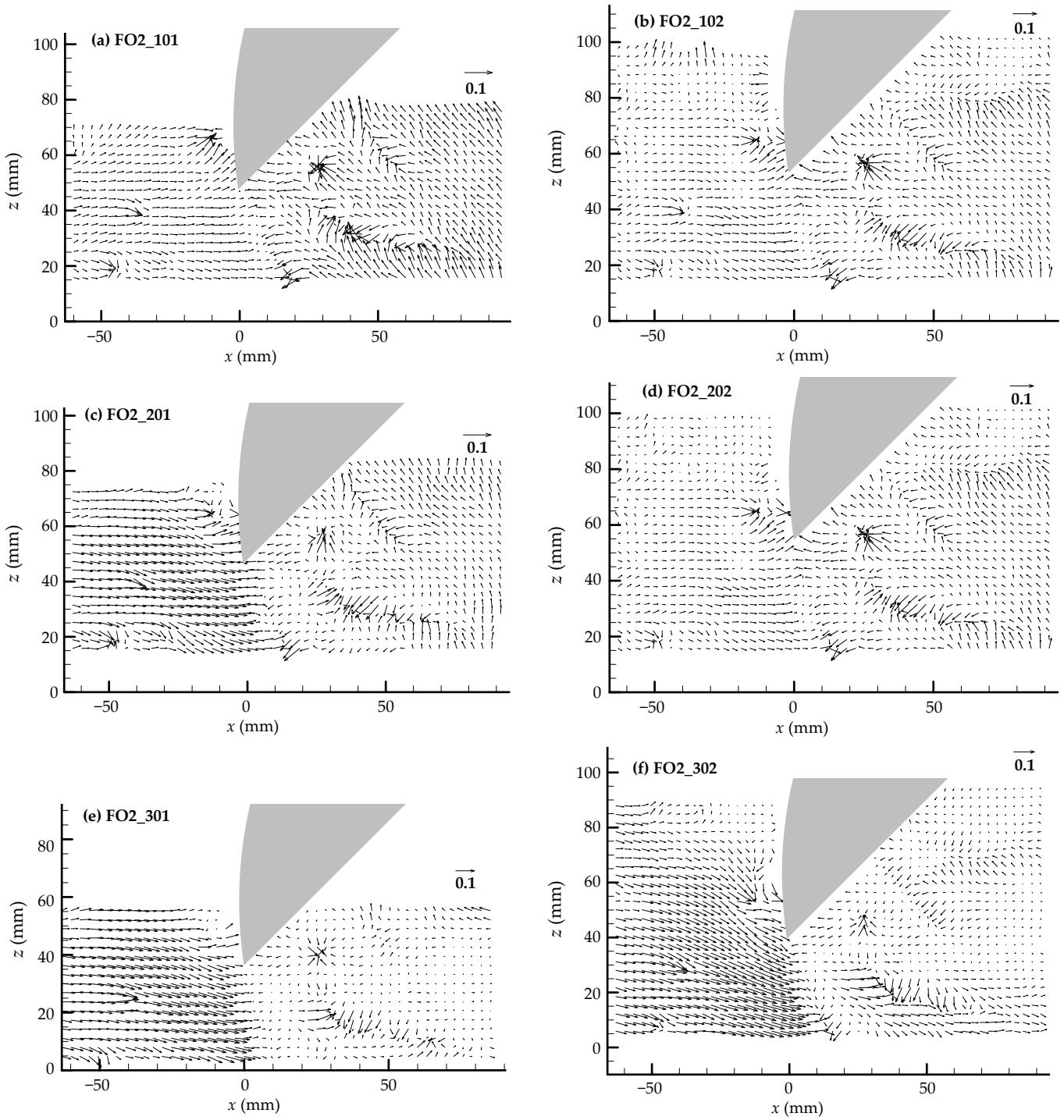

Figure 12. Two-dimensional vector plots near the weir gate mouth (case FO2).

4.2. Turbulence Properties

From the time-averaged velocity values in Figures 11 and 12, the turbulent components in the x- and z-directions were calculated (Figures 13–16), and based on this, the Reynolds shear stress per unit density ($\overline{uw}$) distribution was analyzed (Figures 17 and 18). For the u' distribution, there was a small deviation both upstream and downstream of the gate mouth when the opening was set at 30°, but at 45°, the deviation was larger, with the upstream turbulence component being greater than the downstream component (Figures 13 and 14). Similar patterns were calculated in the w' distribution as well (Figures 15 and 16). The maximum value of w' also occurred, in all cases, near the bottom (x = ~50 mm, z = ~0 mm), where the gate model can be

lowered. This is due to the increasing velocity deviation between the upper and lower layers as the flow approaches the arc-shaped bottom structure of the gate model.

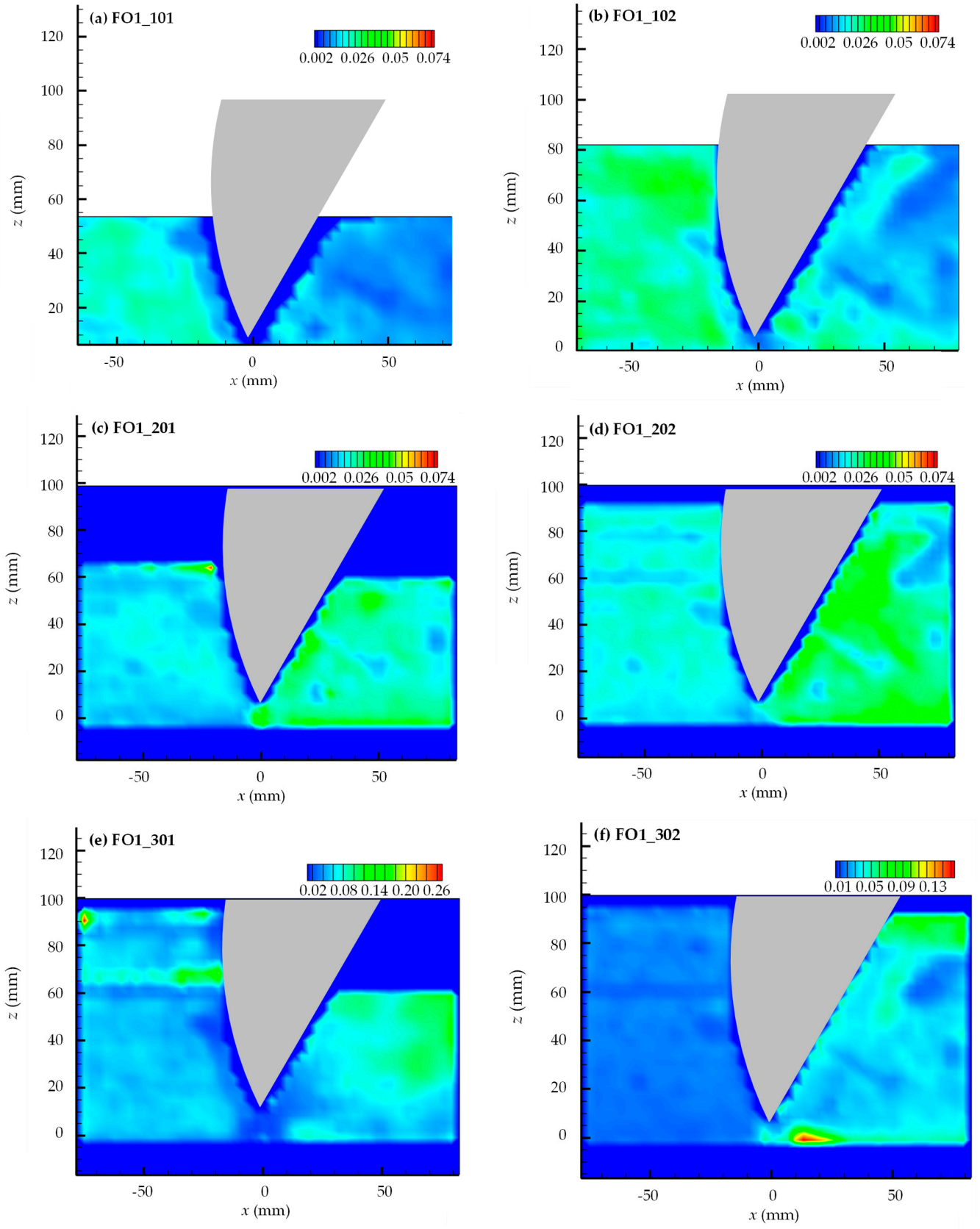

Figure 13. Distribution of streamwise directional turbulence intensity (case FO1).

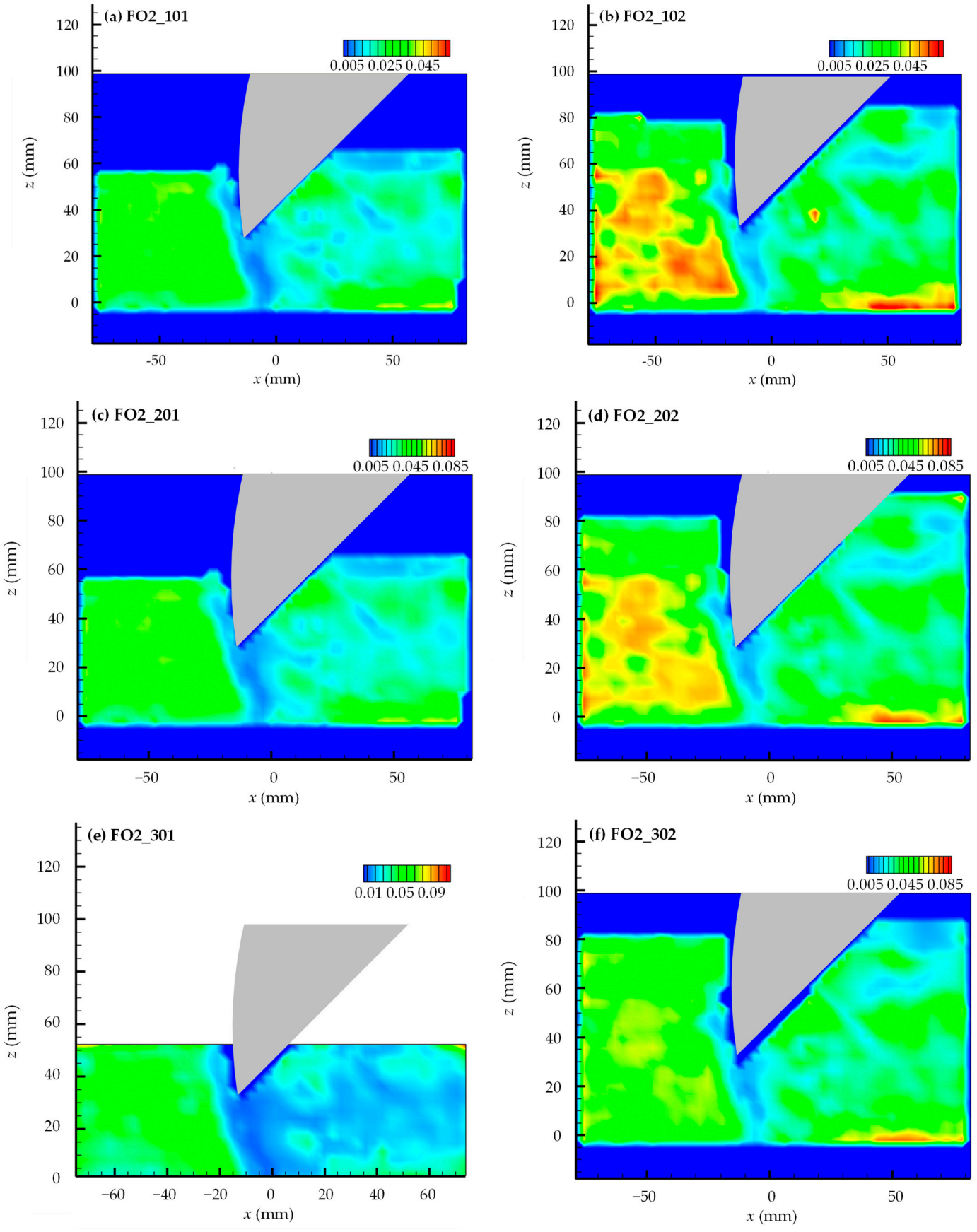

Figure 14. Distribution of streamwise directional turbulence intensity (case FO2).

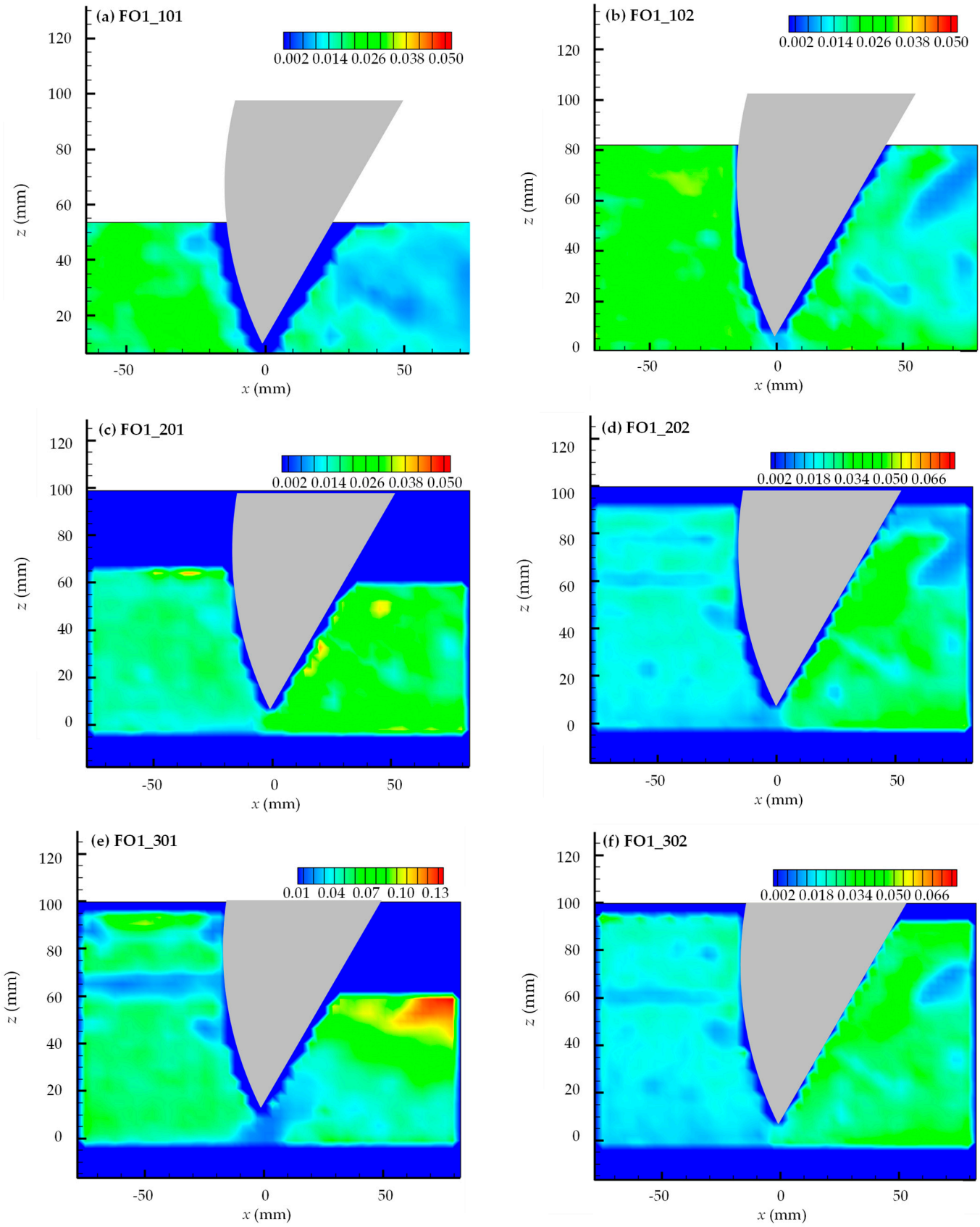

Figure 15. Distribution of depth-wise directional turbulence intensity (case FO1).

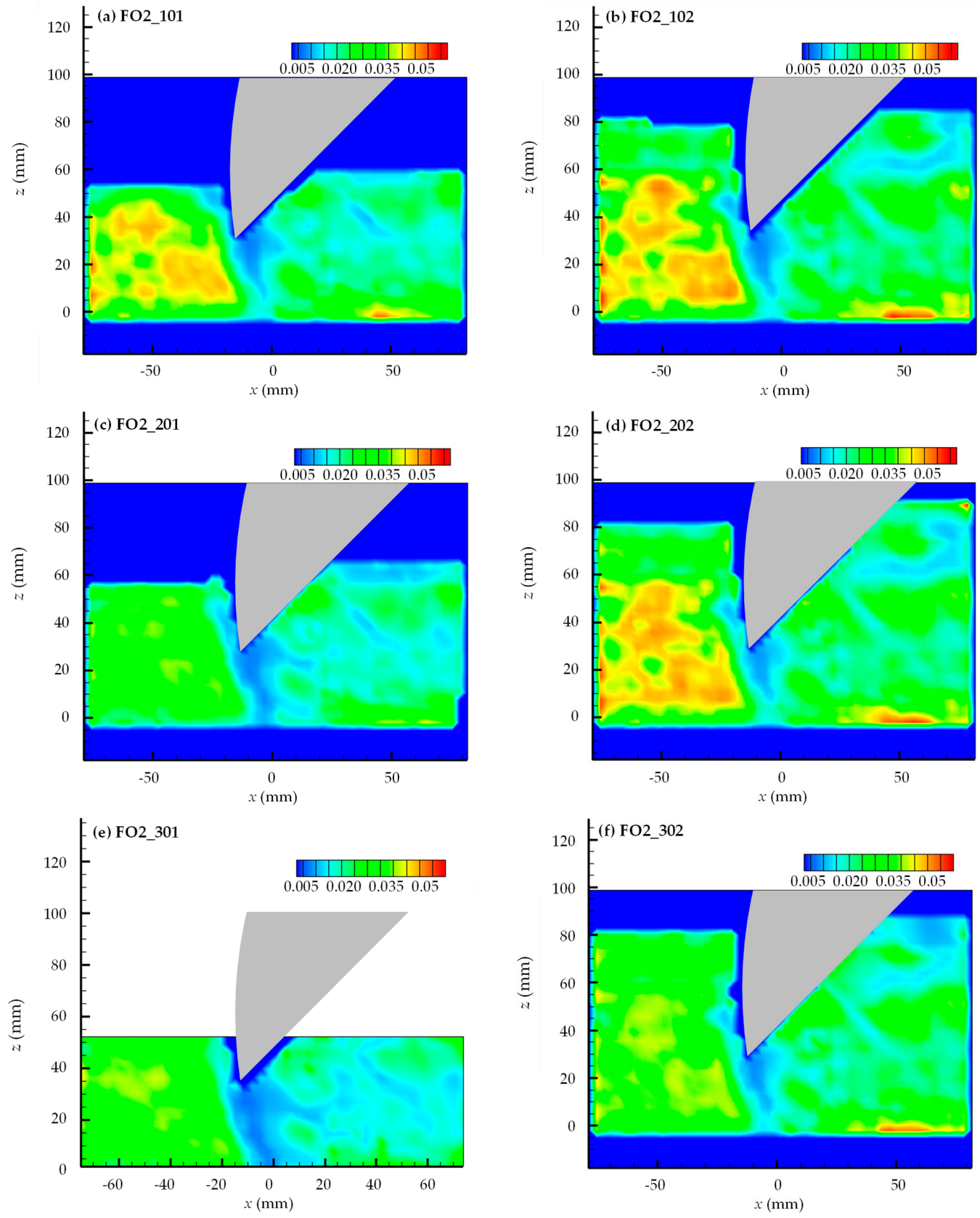

Figure 16. Distribution of depth-wise directional turbulence intensity (case FO2).

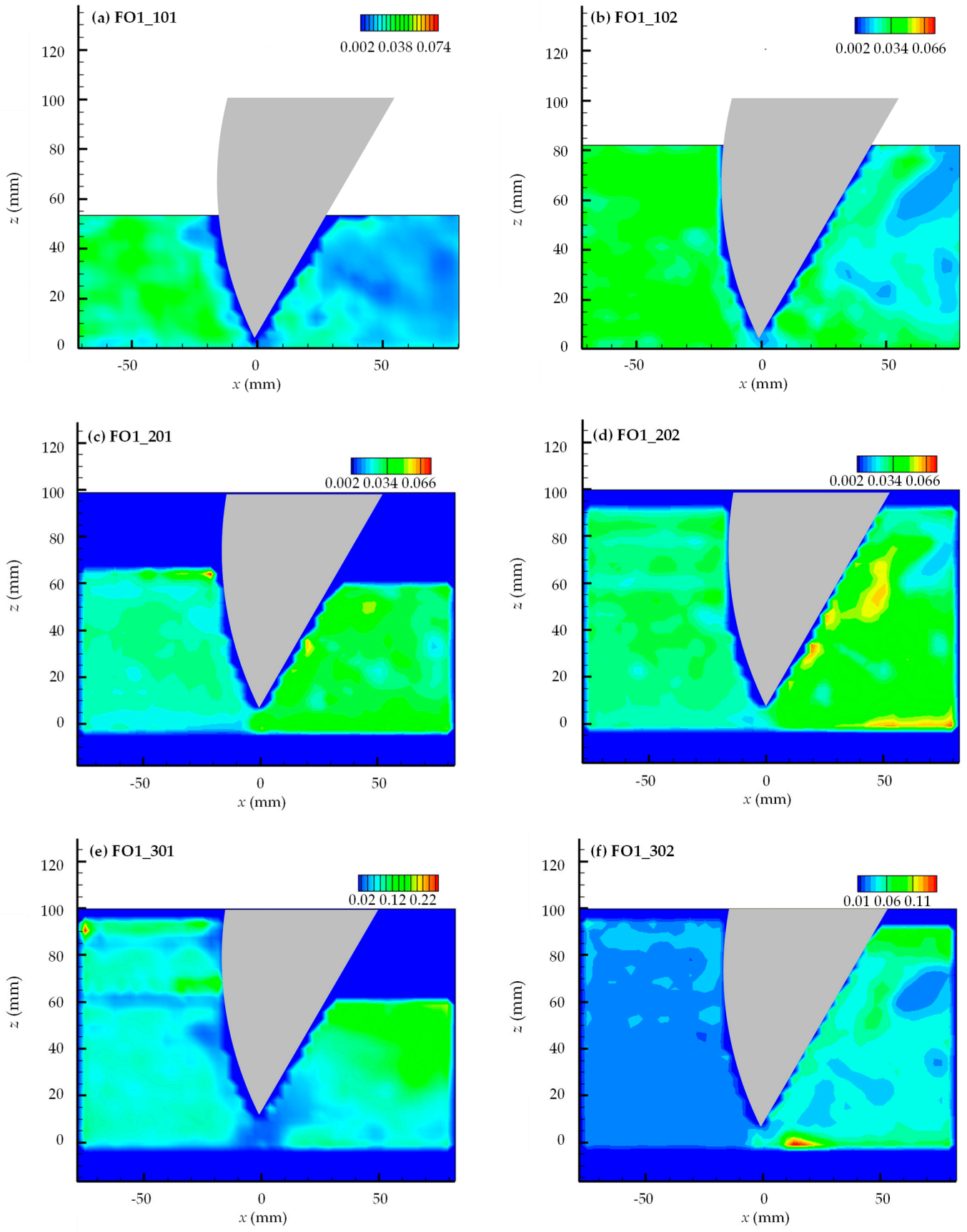

Figure 17. Distribution of Reynolds shear stress per unit density (case FO1).

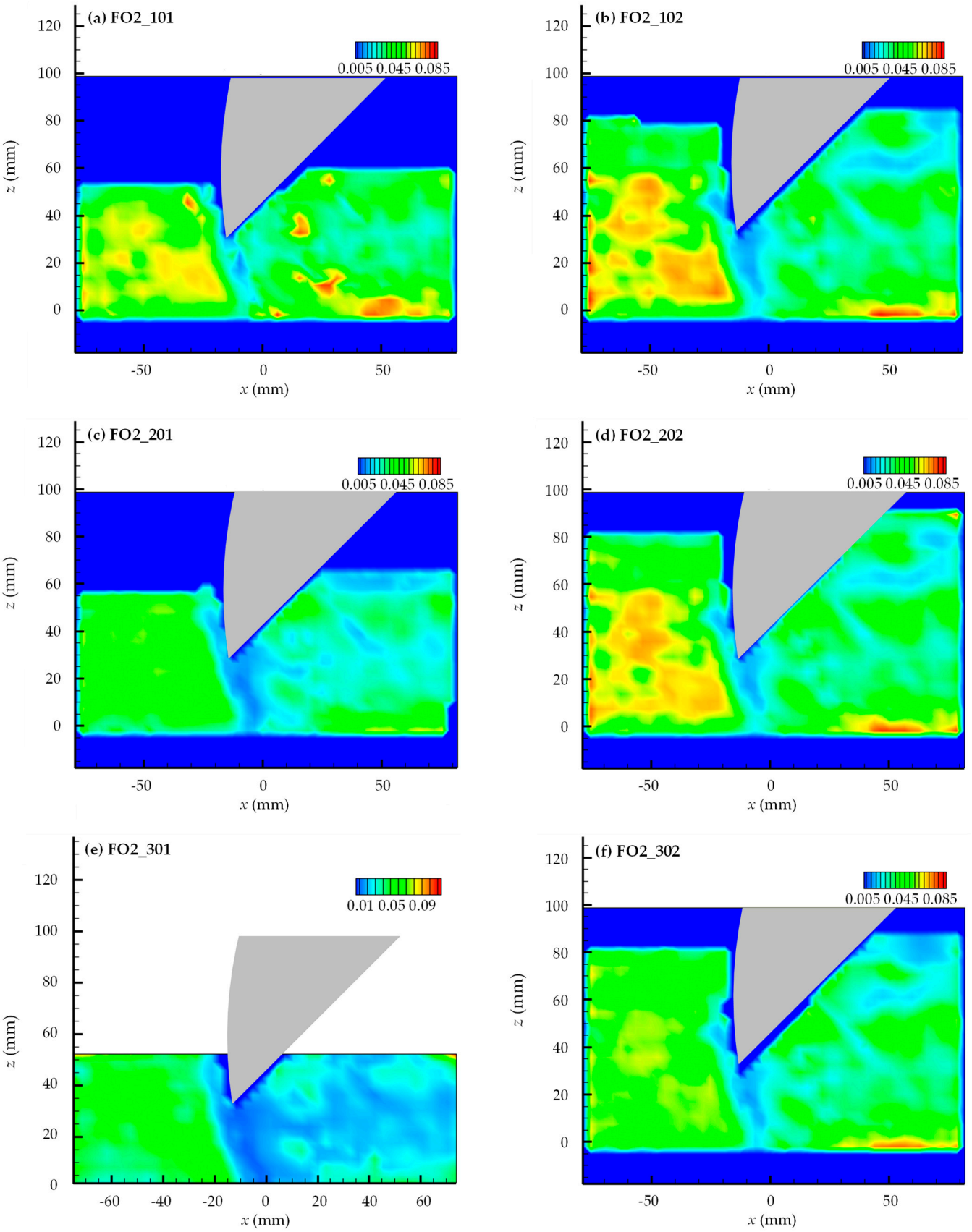

Figure 18. Distribution of Reynolds shear stress per unit density (case FO2).

The Reynolds shear stress measures the additional shear force in a turbulent flow caused by fluctuating velocity components. It reflects how turbulence contributes to the overall shear stress in the fluid, indicating the level of turbulence and momentum transfer between fluid layers. The distributions of the Reynolds shear stress per unit density ($\overline{u'w'}$) in each case are depicted in Figures 17 and 18 using the results of u' and w'. Within the vortex, due to the backward flow pattern, $\overline{u'w'}$ tends to be relatively low. However, at the boundary between the vortex and the primary streamwise directional flow, where a significant velocity deviation occurs, strong mixing can result in an increase in $\overline{u'w'}$. This has some similarities to former research, where the effects of rotational flow in turbulence from generated and dissipated vortices in corrugated pipes were displayed [25–27]. Particularly in the FO1-301 case from Figure 11e, where the characteristics of the backward flow pattern were prominent, the $\overline{u'w'}$ value near the rear of the gate model was calculated to be ~0.15 m^2/s^2, which is about twice that of the other cases in Figures 17 and 18 (=~0.05 m^2/s^2).

4.3. The Vertical Distribution of Flow Velocity at the Gate Mouth

The velocity components passing through the gate mouth in both the x- and z-directions were analyzed for two gate openings, as shown in Figures 19 and 20. In the FO1 cases (30° gate opening), the overall u distribution exhibited depth-wise variation, with the maximum velocity occurring at z = 5 mm. However, near the bottom, u decreased due to bottom friction, a phenomenon that was more pronounced under conditions where h_d = 0.400 m. The distribution of w generally showed negative values, indicating flow toward the channel bottom, except for some points when the flow rate condition was 0.003 m^3/s (Figure 19). This trend was more pronounced in the FO2 cases (45° gate opening). As the gate opening increased, the height of the orifice section of the gate opening increased, resulting in u values approximately half of those in the FO1 cases. However, a rapid increase in u was observed near the maximum z position (z = 54 mm from the model bottom), particularly near the tip of the gate mouth, which is also evident in the vector field shown in Figure 12. The w values in the FO2 cases demonstrated a more distinct pattern compared to the FO1 cases. Specifically, in the upper layer from $z \approx 20$ mm, positive w values were observed, indicating flow toward the water surface, while in the lower layer, negative values of w indicated flow toward the channel bottom.

The value of the turbulent component at the gate mouth is significantly smaller than that of the entire region. Therefore, the flow component was made dimensionless and compared with the Froude number (Fr = $U_0/\sqrt{gh_d}$) of the experimental condition (Figure 20). g (=9.81 m/s^2) is the gravitational acceleration. Specifically, each maximum value of velocity magnitude along the gate mouth was defined as U_{max}, and when this was made dimensionless with U_0, it was observed to gradually decrease as Fr increased (Figure 21). This trend was more clearly illustrated in the FO2 cases than in the FO1 cases. The regression equation for this functional relationship was derived with two characteristic coefficients, as shown in the following equation:

$$\frac{u_{max}}{U_0} = \alpha \ln(\mathrm{Fr}) + \beta \quad (8)$$

where α and β denote the characteristic coefficient and constant term, respectively.

From Figure 21, both values of α and β were estimated with negative values, as shown in Table 2. Based on the observed data, the results of calculating Equation (8) showed that for case FO2, the R^2 value is 0.846, indicating a relatively strong correlation. In contrast, case FO1 yielded a lower R^2 value of 0.274, suggesting a weaker correlation. However, by incorporating a discrepancy ratio line for both cases, the relationship can be demonstrated more clearly. This comparison underscores the consistency of the data despite the lower R^2 value in case FO1. Future studies involving cases with larger Froude number variations, utilizing either 2D or 3D numerical simulations, can be expected to further clarify the trend observed in Equation (8), making the relationship more robust and insightful.

Table 2. Results of regression coefficients of Equation (8).

Case	α	β	R^2
FO1	−3.13	−8.15	0.274
FO2	−2.97	−9.09	0.846

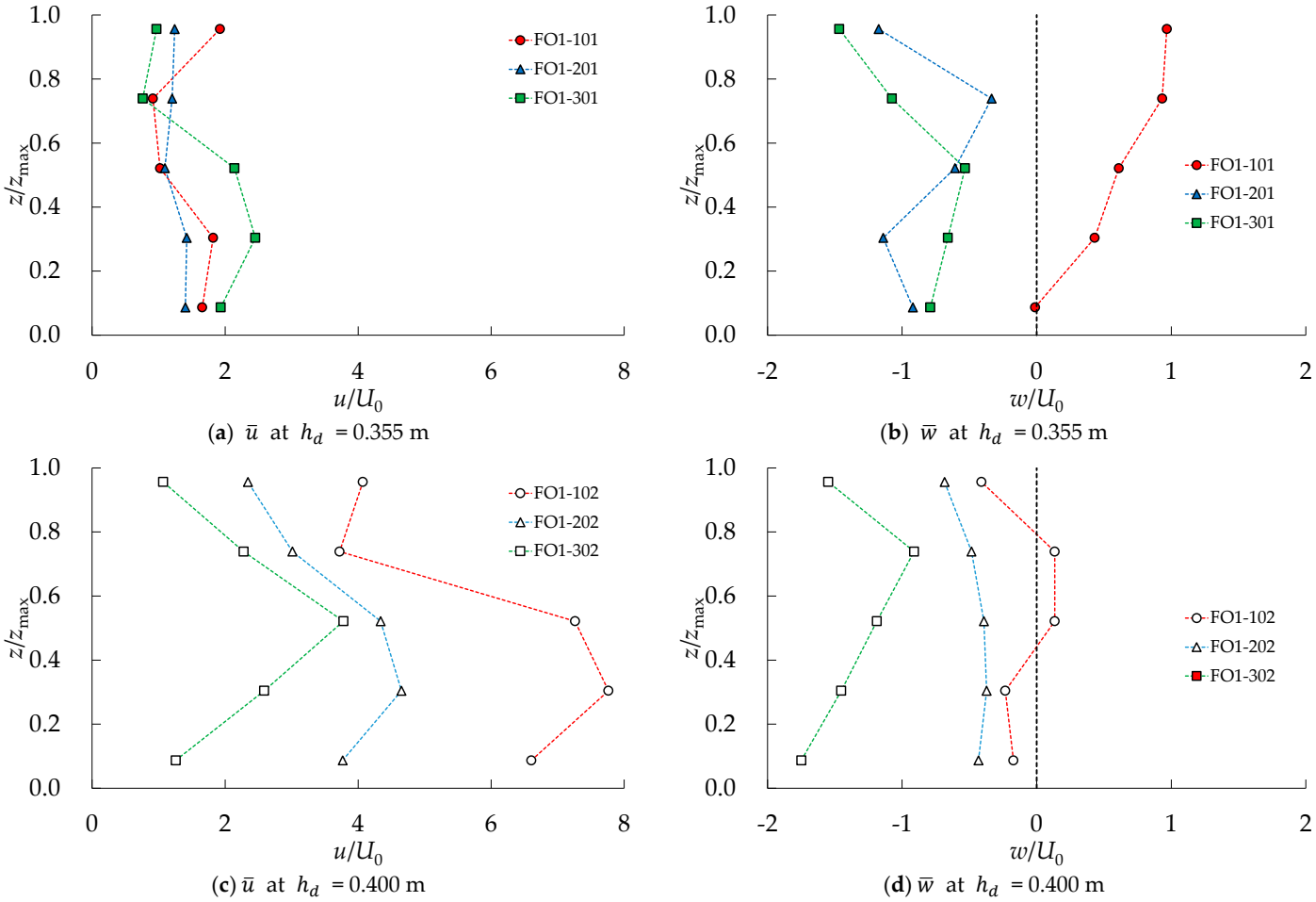

Figure 19. Comparison of dimensionless time-averaged flow velocity at the gate mouth (case FO1).

4.4. Spatial Variation in Depth-Averaged Relative Turbulence Intensity Along the Flow Direction

The flow and turbulence characteristics mentioned in Section 2.2, which can be simultaneously quantified using r_0, were plotted according to the streamwise location (Figure 22). The results indicate that both FO1 and FO2 cases show minimum values about 10 mm downstream from the gate mouth. In the FO1 cases, the values increased in the downstream region compared to the upstream, while in the FO2 cases, the downstream values were reduced by up to about 50% compared to the upstream. Therefore, it can be concluded that the 45-degree gate opening is more effective than the 30-degree gate opening in terms of turbulent energy dissipation.

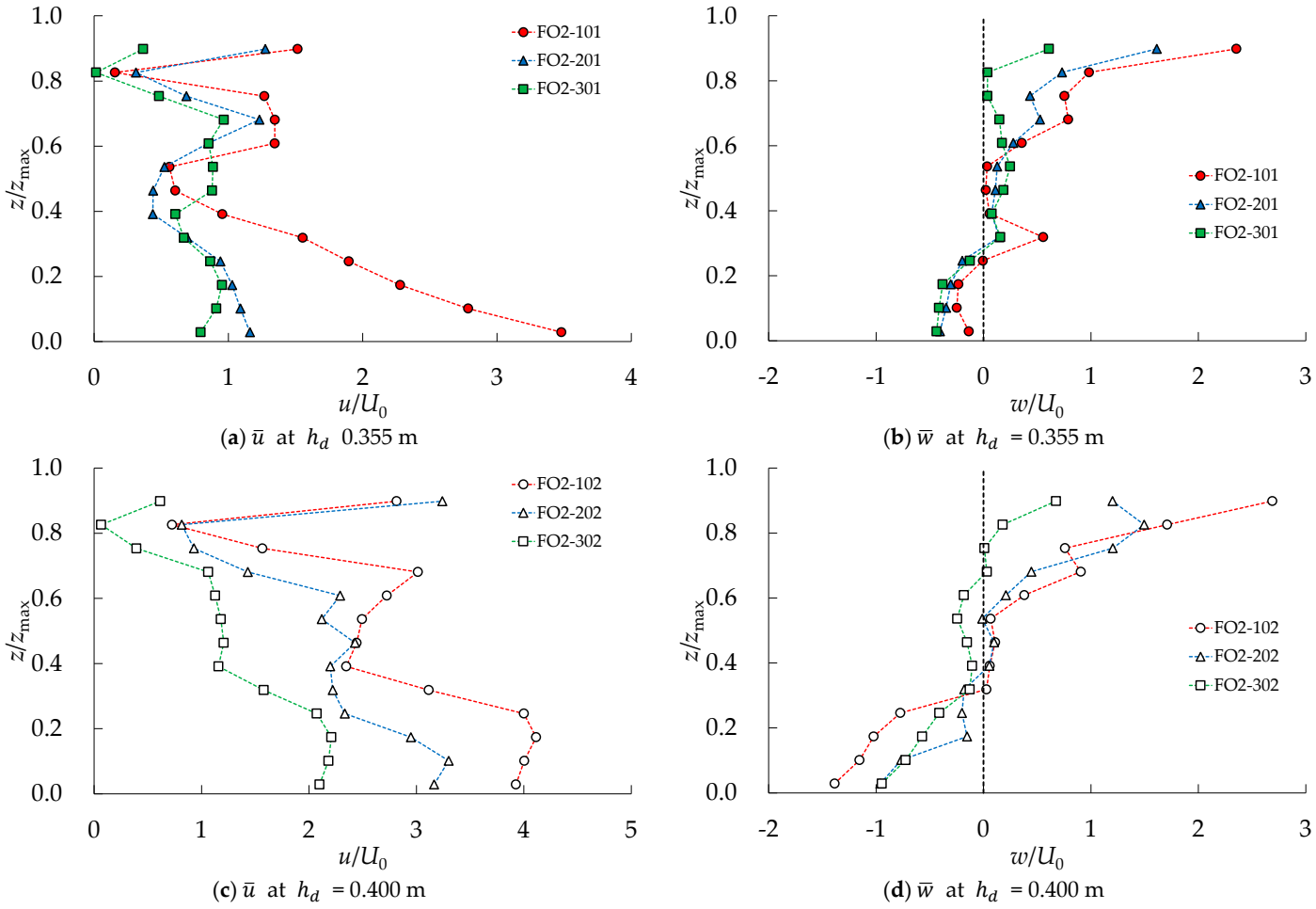

Figure 20. Comparison of dimensionless time-averaged flow velocity at the gate mouth (case FO2).

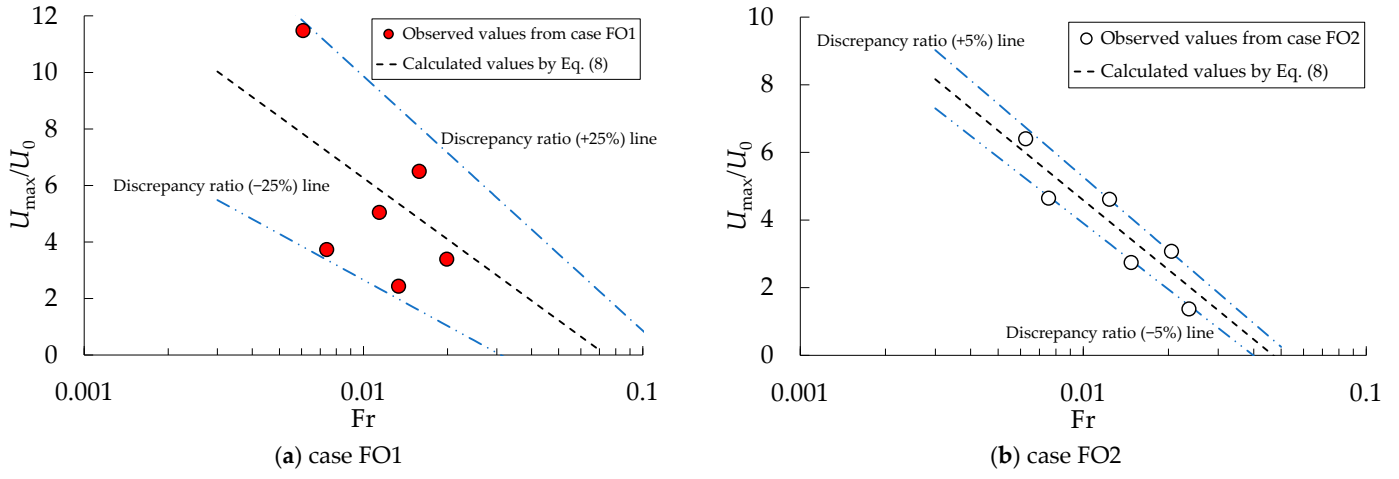

Figure 21. The functional relationship between the Froude number and dimensionless maximum velocity at the gate mouth.

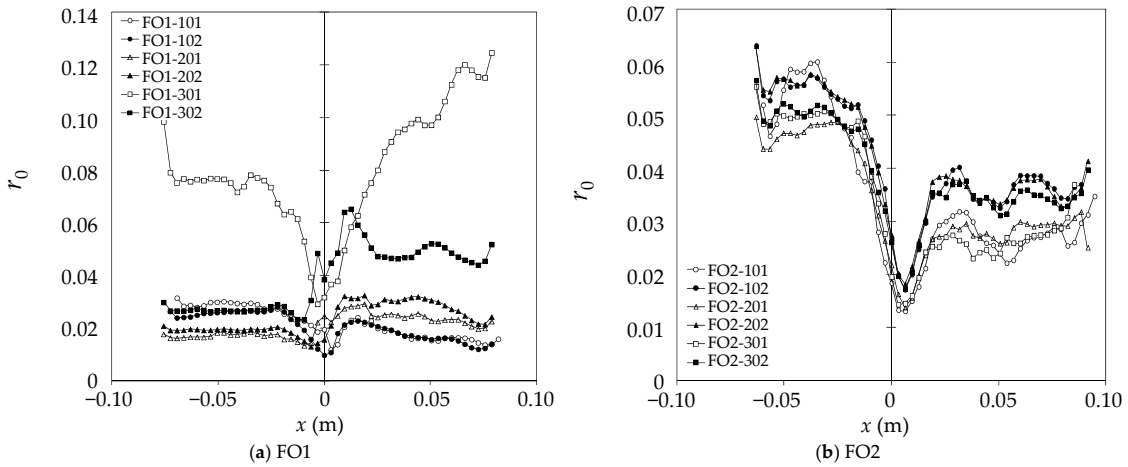

Figure 22. Longitudinal distribution of depth-averaged relative turbulence intensity.

5. Summary and Conclusions

This study investigated the hydraulic behavior and turbulent flow characteristics around a rising sector gate under the undershot operation condition, focusing on the effect of various flow rates, downstream water levels, and gate-opening angles. Experiments were conducted in a laboratory flume equipped with advanced measurement systems, such as Particle Image Velocimetry (PIV), to capture high-resolution velocity and turbulence data in the vicinity of the gate. A detailed analysis of time-averaged flow velocities, turbulence intensities, and Reynolds shear stress was carried out to better understand the flow behavior under different experimental conditions.

The study focused on four primary objectives:

- Flow Velocity Distribution: The velocity distribution near the gate opening revealed significant variations depending on the upstream discharge and downstream water surface elevation. In particular, the flow velocity at the gate mouth was considerably higher than the average cross-sectional velocity, which could contribute to increased shear stress on the gate structure. The experimental results demonstrated that the highest velocities were observed near the bottom of the gate opening, particularly in the 30° and 45° gate-opening scenarios.
- Turbulence Characteristics: The turbulence intensity was analyzed using depth-averaged turbulence energy and the Reynolds shear stress distribution. The results indicated that the turbulence intensity was higher near the boundary between the gate mouth and the upstream section, especially at greater flow rates. Additionally, the flow structure downstream of the gate exhibited prominent vortex formations, which were more pronounced with larger gate openings and higher flow rates.
- Reynolds Shear Stress: The distribution of Reynolds shear stress per unit density showed that the highest shear stress occurred near the bottom of the gate opening, where flow separation and high turbulence were observed. The experimental data indicated that the turbulence-induced shear stress was significantly affected by both the gate-opening angle and the upstream discharge conditions.
- Impact of Gate-Opening Angle: The gate-opening angle had a substantial impact on the flow regime. In the 45° gate-opening condition, the velocity and turbulence intensity were generally lower than in the 30° opening, but the vertical flow distribution showed greater depth-wise variation. This suggests that the larger gate opening provides a more uniform flow distribution but also allows for more complex turbulence structures near the gate mouth.

The findings of this research provide valuable insights into the flow and turbulence characteristics of rising sector gates in undershot operation. Several key conclusions can be drawn from the experimental analysis:

- Flow Velocity and Shear Stress: This study revealed that flow velocity and shear stress are significantly concentrated near the bottom of the gate opening. This concentration of forces poses potential risks for structural wear and failure, highlighting the importance of the design and maintenance of gate structures in practical applications of fields.
- Turbulence Intensity and Vortex Formation: The turbulence intensity and formation of vortices downstream of the gate were found to increase with higher flow rates and larger gate openings. These flow structures can influence sediment transport and downstream erosion, which is crucial for the design of hydraulic structures aimed at flood control and sediment management.
- Gate Design Implications: The results emphasize the need for precise control of gate operations to balance flow regulation, sediment flushing, and structural integrity. In particular, the findings suggest that the 45° gate-opening angle is more efficient in minimizing turbulence intensity while maintaining effective water discharge, making it a suitable decision for scenarios requiring moderate flow control and sediment flushing upstream of the movable weir gate.

Although this study provides a detailed analysis of flow and turbulence properties, further research is needed to explore the long-term effects of repeated gate operations on structural stability. Additionally, future studies could incorporate three-dimensional flow modeling to gain a more comprehensive understanding of the complex flow dynamics associated with various gate designs.

Author Contributions: C.G.S. was responsible for conceptualization, methodology, and software application in this research. J.S. and S.W.P. were involved in model validation, data curation, and writing—original draft preparation. S.W.P. and C.G.S. were involved in writing—review and editing. C.G.S. contributed to supervision, project administration, and funding acquisition. All authors have read and agreed to the published version of the manuscript.

Funding: This work was supported by the Korea Environment Industry & Technology Institute (KEITI) through the R&D Program for Innovative Flood Protection Technologies against Climate Crisis Project, funded by the Korea Ministry of Environment (MOE) (2022003470001).

Data Availability Statement: The data presented in this study are available on request from the corresponding author. The data are not publicly available due to the substantial size of data volume.

Conflicts of Interest: The authors declare no conflicts of interest.

Appendix A

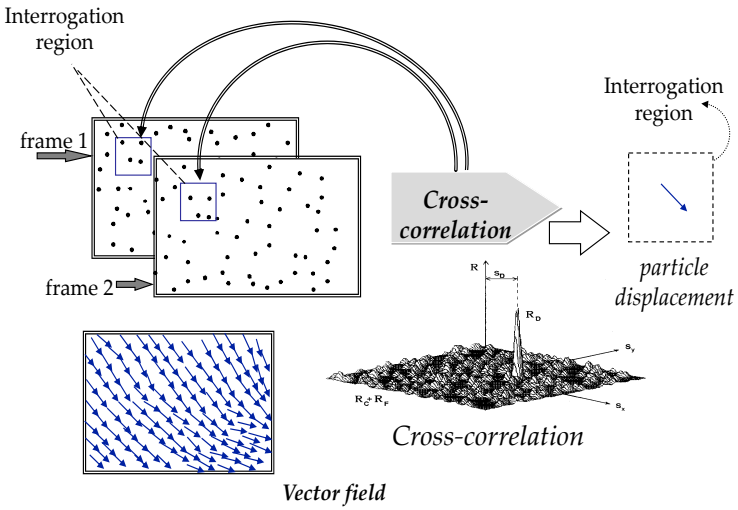

Figure A1. Schematic diagram of cross-correlation processing in the PIV measurement.

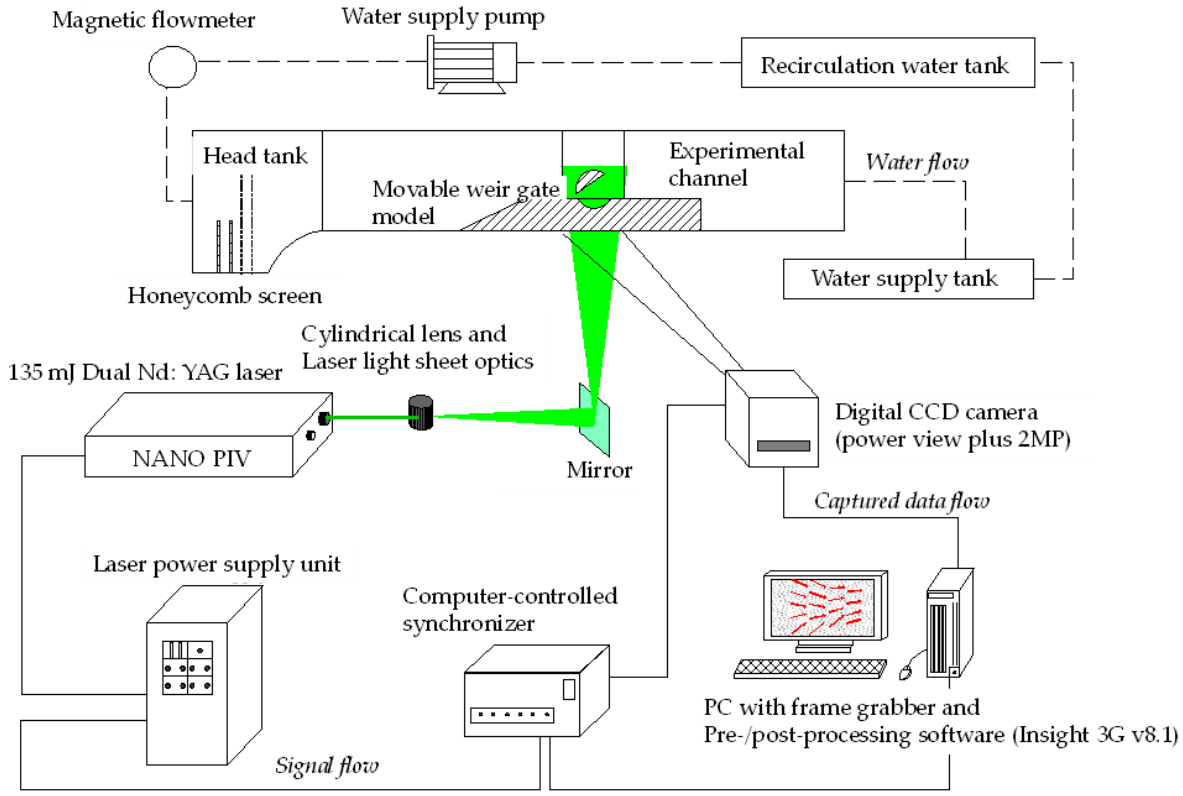

Figure A2. A schematic diagram of the water, signal, and data flow in the experimental channel with the PIV measuring system.

References

1. Raffel, M.; Willert, C.E.; Scarano, F.; Kähler, C.J.; Wereley, S.T.; Kompenhans, J. *Particle Image Velocimetry: A Practical Guide*; Springer: Berlin/Heidelberg, Germany, 2018. [CrossRef]
2. Swamee, P.K. Sluice-gate Discharge Equations. *J. Irrig. Drain. Eng.* **1992**, *118*, 57–60. [CrossRef]
3. Rajaratnam, N.; Subramanya, K. Flow equation for the sluice gate. *J. Irrig. Drain. Div.* **1967**, *93*, 167–186. [CrossRef]
4. Ackers, A.; White, W.R.; Perkins, J.A.; Harrison, A.J.M. *Weirs and Flumes for Flow Measurements*, 1st ed.; John Wiley & Sons: New York, NY, USA, 1978.
5. Swamee, P.K. Generalized Rectangular Weirs equations. *J. Hydraul. Eng.* **1988**, *114*, 945–949. [CrossRef]
6. BSI. Thin-plate Weirs and Venturi Flumes. In *Methods of Measurement of Liquid Flow in Open Channel BSI 3680-4A*; British Standard Institution: London, UK, 1981. [CrossRef]
7. Peterka, A.J. *Hydraulic Design of Stilling Basins and Energy Dissipators*; Department of the Interior, Bureau of Reclamation: Washington, DC, USA, 1978.
8. United States Department of the Interior Bureau of Reclamation. *Design of Small Dams*; US Department of the Interior, Bureau of Reclamation: Washington, DC, USA, 1987.
9. United States Department of the Interior Bureau of Reclamation. *Hydraulic Laboratory Techniques*, 2nd ed.; Bureau of Reclamation, U.S. Department of the Interior: Denver, CO, USA, 1980.
10. Dehghani, A.A.; Bashiri, H. Experimental Investigation of Scouring in Downstream of Combined Flow over Weirs and below Gates. In Proceedings of the 33rd IAHR Conference, Vancouver, BC, Canada, 9–14 August 2009; pp. 3604–3609.
11. Sihag, P.; Nouri, M.; Ahmadpari, H.; Seyedzadeh, A.; Kisi, O. Approximation of the Discharge Coefficient of Radial Gates Using Metaheuristic Regression Approaches. *Sustainability* **2022**, *14*, 15145. [CrossRef]
12. Chanson, H.; Montes, J.S. Overflow Characteristics of Circular Weirs: Effects of Inflow Conditions. *J. Irrig. Drain. Eng. ASCE* **1998**, *124*, 152–162. [CrossRef]
13. Clemmens, A.J.; Strelkoff, T.S.; Replogle, J.A. Calibration of Submerged Radial Gates. *J. Hydraul. Eng.* **2003**, *129*, 680–687. [CrossRef]
14. Cassan, L.; Belaud, G. Experimental and numerical investigation of flow under sluice gates. *J. Hydraul. Eng.* **2012**, *138*, 367–373. [CrossRef]
15. Kubrak, E.; Kubrak, J.; Kiczko, A.; Kubrak, M. Flow measurements using a sluice gate; analysis of applicability. *Water* **2020**, *12*, 819. [CrossRef]
16. Gharahgezlou, M.; Masoudian, M.; Kordi, E.; Sahin, B.; Azimi, A.H. Free flow over and under cylindrical weir-gates with a flow extender. *ISH J. Hydraul. Eng.* **2024**, *30*, 171–184. [CrossRef]

17. Zhang, S.; Wang, X.; Ma, H. Operating Force Characteristics of Sector Gates Based on Prototype Testing. *Water* **2024**, *16*, 762. [CrossRef]
18. Hoffmans, G.J. *The Influence of Turbulence on Soil Erosion*; Eburon Uitgeverij BV: Delft, The Netherlands, 2012; Volume 10.
19. Nezu, I.; Nakagawa, H. *Turbulence in Open-Channel Flows*; IAHR-Monograph: Beijing, China, 1993.
20. Howarth, M.J.; Souza, A.J. Reynolds stress observations in continental shelf seas. *Deep Sea Res. Part II Top. Stud. Oceanogr.* **2005**, *52*, 1075–1086. [CrossRef]
21. Simpson, J.H.; Williams, E.; Brasseur, L.H.; Brubaker, J.M. The impact of tidal straining on the cycle of turbulence in a partially stratified estuary. *Cont. Shelf Res.* **2005**, *25*, 51–64. [CrossRef]
22. Shig, L.; Babin, V.; Shnapp, R.; Fattal, E.; Liberzon, A.; Bohbot-Raviv, Y. Quadrant analysis of the Reynolds shear stress in a two-height canopy. Flow. *Turbul. Combust.* **2022**, *111*, 35–57. [CrossRef]
23. Haga, K.; Terada, A.; Kaminaga, M.; Hino, R. *Water Flow Experiment Using the PIV Technique and the Thermal Hydraulic Analysis on the Cross-Flow Type Mercury Target Model*; ETDEWEB: Oak Ridge, TN, USA, 2001; Volume 2, pp. 1293–1303.
24. Felice, F.D.; Pereira, F. Developments and Applications of PIV in Naval Hydrodynamics. In *Particle Image Velocimetry. Topics in Applied Physics*; Springer: Berlin/Heidelberg, Germany, 2007; Volume 112, pp. 475–503. [CrossRef]
25. Calomino, F.; Tafarojnoruz, A.; De Marchis, M.; Gaudio, R.; Napoli, E. Experimental and numerical study on the flow field and friction factor in a pressurized corrugated pipe. *J. Hydraul. Eng.* **2015**, *141*, 04015027. [CrossRef]
26. Yoosefdoost, A.; Lubitz, W.D. Sluice Gate Design and Calibration: Simplified Models to Distinguish Flow Conditions and Estimate Discharge Coefficient and Flow Rate. *Water* **2022**, *14*, 1215. [CrossRef]
27. Salmasi, F.; Abraham, J. *Hydraulic Performance of Sluice Gates: A Review of Head Loss Estimation and Discharge Coefficients for Optimal Flow Control and Design Considerations*; IntechOpen: London, UK, 2023. [CrossRef]